

# 基于荧光成像技术的土壤芳香烃总量快速检测方法

石高勇<sup>1,2,3</sup>, 杨瑞芳<sup>2,3\*</sup>, 赵南京<sup>2,3\*\*</sup>, 刘梁晨<sup>1,2,3</sup>, 杨金强<sup>1,2,3</sup>, 黄朋<sup>2,3,4</sup>, 殷高方<sup>2,3</sup>, 方丽<sup>2,3</sup>, 刘文清<sup>2,3</sup>

<sup>1</sup>中国科学技术大学环境科学与光电技术学院, 安徽 合肥 230026;

<sup>2</sup>中国科学院合肥物质科学研究院安徽光学精密机械研究所环境光学与技术重点实验室, 安徽 合肥 230031;

<sup>3</sup>安徽省环境光学监测技术重点实验室, 安徽 合肥 230031;

<sup>4</sup>合肥学院生物食品与环境学院, 安徽 合肥 230601

**摘要** 针对土壤芳香烃总量快速检测难题,研究了基于荧光成像技术的土壤芳香烃荧光信号获取、特征提取方法和质量分数总量反演的方法。基于发光二极管(LED)紫外激发光源、面阵CCD相机、透镜等器件搭建了实验系统,获得了最佳光源激发能量、激发角度等参数,并对实验系统检测能力进行了分析。利用这一实验系统获取了质量分数范围为 $0\sim 25000\times 10^{-6}$ 的标准土壤中机油的系列荧光图像,基于高斯降噪处理和最大类间方差法研究了图像噪声抑制与荧光信号提取方法,建立了标准土壤中机油芳香烃总量的反演模型,并利用反演模型对待测样本的机油芳香烃总量进行了预测。结果表明:总量反演模型的决定系数( $R^2$ )达到了0.9889,检测限为82.18,对20个样品测试的误差基本在12%以内。

**关键词** 测量; 土壤; 荧光成像; 多环芳烃; 相机; 图像处理

中图分类号 X53

文献标志码 A

DOI: 10.3788/AOS221436

## 1 引言

随着石油化工和相关产业的迅速发展,场地石油污染事件频发。芳香烃苯系物<sup>[1]</sup>和多环芳烃<sup>[2]</sup>是石油的主要成分,具有致畸、致癌、致基因突变的三致效应,一旦进入土壤会在其中长期积累,最终会通过食物链影响人体健康<sup>[3]</sup>。

有机污染物传统检测技术主要有气相色谱法<sup>[4]</sup>、气相色谱-质谱法<sup>[5-6]</sup>和液相色谱法<sup>[7]</sup>等,虽然这些方法是标准方法,且灵敏度高、准确性好,但是有着样品预处理复杂、测试速度慢和分析成本高等缺点,故不适用于场地快速检测。有机污染物光学检测方法具有样品使用少、预处理简单和快速无损的优点,其已被用于土壤有机污染物检测中。Li等<sup>[8]</sup>建立了气相色谱-火焰离子化检测器结合高效10 m短色谱柱测定总石油烃的高效方法,该方法可以很好地满足相关风险评估和环境监测的需求。张世芝等<sup>[9]</sup>利用紫外光谱法和化学计量学方法建立了水样中苯甲酸、苯酚和苯胺的同时测定方法,在独立测试集上三组分的预测误差均方根分别为0.9716、0.7938、0.7652。孟凡昊等<sup>[10]</sup>采用自主研发的差分吸收光谱系统对合肥市交通主干道上的

苯、甲苯、间二甲苯和邻二甲苯进行了连续观测,观测期间上述苯系物的平均质量浓度分别为21.7、63.6、33.9、98.7  $\mu\text{g}/\text{m}^3$ ,并结合观测期间的风速风向、甲苯与苯的特征比值,以及与CO等污染物的相关性,计算得出苯、甲苯与CO的相关性系数分别为0.55和0.40。王玉涛等<sup>[11]</sup>选取同步荧光光谱得到的指标对土壤水溶性有机物的来源和结构进行了评估,相比于单一激发光谱和发射光谱,同步荧光光谱能够提供更高的灵敏度和更好的选择性。庞燕华等<sup>[12]</sup>使用三维荧光光谱和紫外-可见分光光度技术研究了温度对土壤有机物的结构和组分的影响,发现土壤有机物的芳香性和疏水性会随着温度的增加而不断降低。Douglas等<sup>[13]</sup>基于烷烃和多环芳烃的可见-近红外信号,使用偏最小二乘回归和随机森林建立校正模型,发现近红外光谱结合随机森林校准模型的预测性能优于偏最小二乘回归。吴嘉鹏等<sup>[14]</sup>分别使用紫外法和红外法测定了石油烃,二者的精密度和准确度等性能指标相近,紫外分光光度法对较复杂水体石油类样品的测定存在局限性。

目前已有的光学检测技术主要针对有机物组分进行检测,而测量的组分误差较大,不能通过简单求和得

收稿日期: 2022-07-07; 修回日期: 2022-07-29; 录用日期: 2022-08-09; 网络首发日期: 2022-08-19

基金项目: 国家重点研发计划子课题(2020YFC1807204-1)、中国科学院科技服务网络计划(STS计划)区域重点项目(KFJ-STQYD-2021-04-001-4)、安徽省重点研究和开发计划(201904a07020089)

通信作者: \*rfyang@aiofm.ac.cn; \*\*njzhao@aiofm.ac.cn

到有机物总量,成像技术为实现土壤有机污染物的总量检测提供了一种可选途径。本文搭建了紫外诱导荧光成像系统,研究了标准土壤(GBW0749415)中机油(15W-40)芳香烃总量的直接检测方法,为实现土壤芳香烃总量的场地快速测定提供了一种可行方案。

## 2 材料和方法

### 2.1 实验系统搭建

汽油、柴油和原油的标准三维荧光光谱如图 1 所

示,在 280 nm 左右时激发最佳,且该波长处可以有效避免激发土壤中有机质的荧光,从而可避免有机质荧光对石油类污染物荧光信号的干扰。发光二极管(LED)具有波长范围覆盖大、能耗低、稳定性好和环境适应能力强等优点,适用于场地土壤石油芳香烃总量的检测。因此,实验系统采用了波长为 280 nm 的低功耗、高强度紫外 LED 作为激发光源,其光谱曲线如图 2 所示。

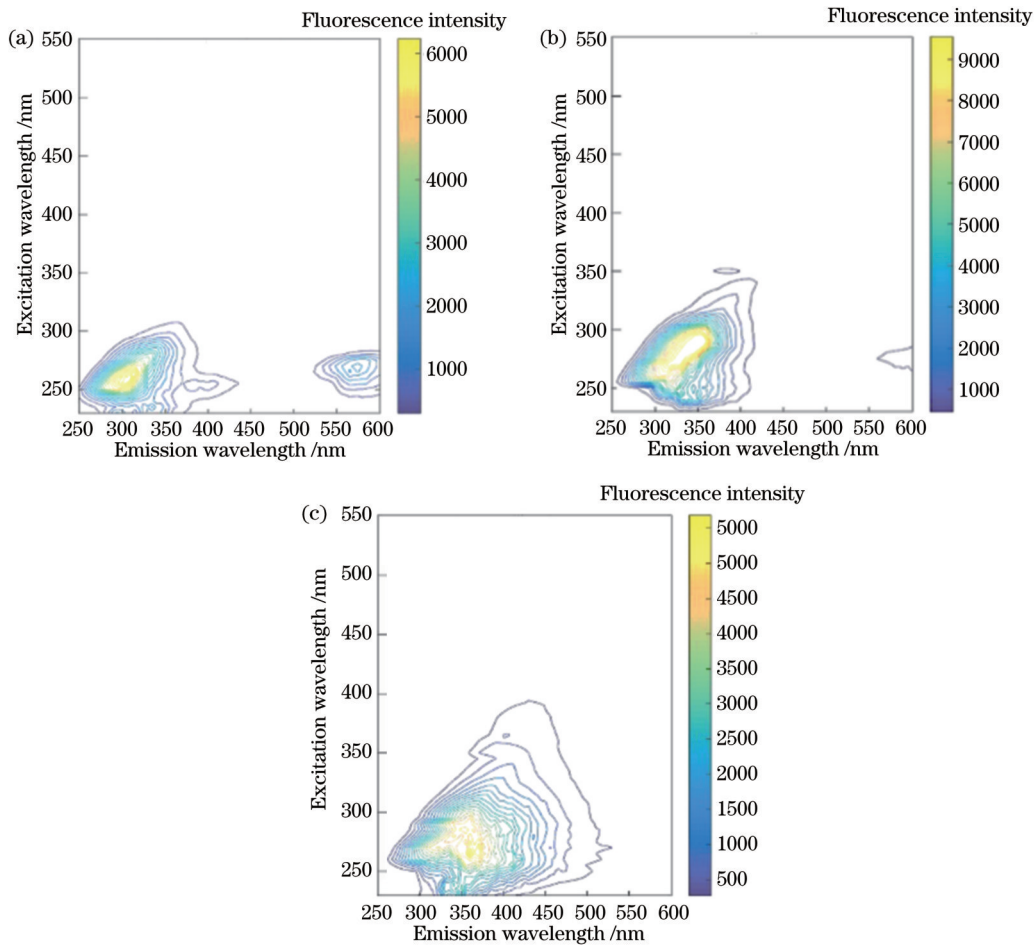


图 1 油类的三维荧光光谱。(a)汽油;(b)柴油;(c)原油

Fig. 1 Three-dimensional fluorescence spectra of oils. (a) Gasoline; (b) diesel fuel; (c) crude

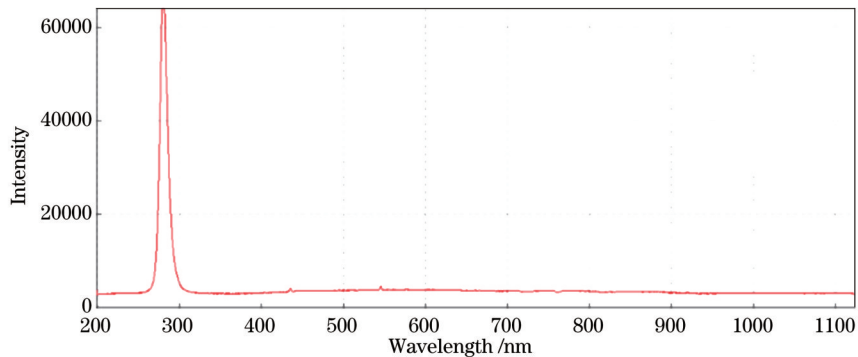


图 2 280 nm 紫外光源光谱曲线

Fig. 2 Spectral curve of 280 nm ultraviolet light source

CCD 相机具有体积小、质量轻、功耗小和工作电压低等优点,且在分辨率、灵敏度等方面具有优越性,因此本系统采用面阵 CCD 相机作为光电探测器来检测荧光图像信号,其响应范围为 200~1000 nm,如图 3 所示。荧光信号本身较弱,且激发光和环境光对其干扰很大,故对于从复杂的背景中提取到的荧光信号,需

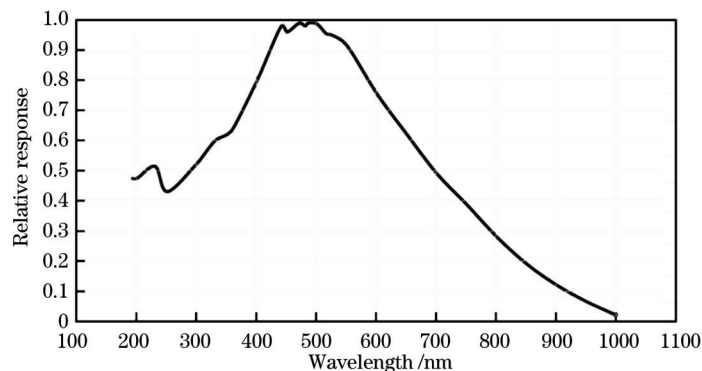


图 3 CCD 相机的光谱响应范围曲线

Fig. 3 Spectral response range curve of CCD camera

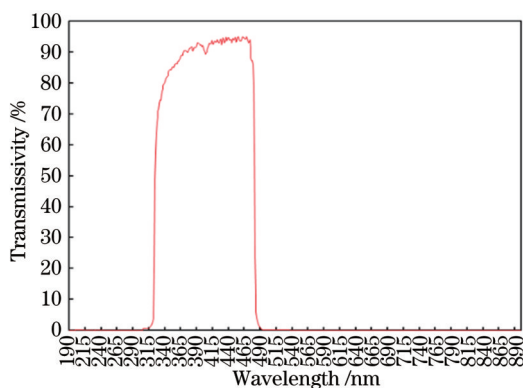


图 4 滤光片的透射率

Fig. 4 Transmissivity of filter

搭建实验系统示意图如图 5 所示,检测系统包括 LED 激发光源、平凸透镜、滤光片、CCD 相机、样品架、控制电路板和个人计算机(PC),其中  $f$  为焦距。来自 LED 光源的激发光经过透镜组准直会聚后,以一定大小的光斑照射在土壤样品表面,从而激发土壤中的石油芳香烃产生荧光。CCD 相机捕获荧光图像信号后,将信号传输至计算机中进行分析处理。搭建系统过程中优化了系统参数:1)调整各个器件的间距使光源照射到土壤上的能量尽可能大;2)增加了照射到土壤上的光斑大小,并调整光圈和焦距,以获取清晰图像。

## 2.2 样品制备

选择标准土壤(GBW07494)来配制机油(15W-40)实验样品,配制过程为称取 285 g 的土壤粉末放置于烧杯中,向里面加入 15 g 机油和少量无水乙醇搅拌均匀,并置于烘箱内烘干,制成含有 5% 质量分数机油的土壤。在烘干时,设置烘箱的温度为 40 °C,高于机油的沸点,此时无水乙醇挥发,仅留下了机油中的有机

要去除杂散光的影响。选择性能优越的带通滤光片(FF01-405)置于相机镜头前方,只允许被测样品发射的荧光透过而阻止激发光、环境光和其他杂散光通过,从而获得具有理想信号波长的激发光和荧光。图 4 为所用滤光片的透过率曲线。

物。向质量分数为 5% 的样品中加入一定量的空白土样来实现低质量分数样品的制作,如表 1 所示,其中 Blank 为加入的空白土壤质量。

在配制过程中,需要对混合过的样品使用搅拌机进行搅拌和研磨,使其混合均匀。配制好的土壤样品的表面不均匀,这会导致获取到的荧光信号不稳定,故需要使用压片机对土壤粉末进行压片处理。在压片过程中,统一使用了 6 MPa 的压力,每个质量分数的土壤片制备 3 个,其实物图如图 6 所示。实验发现,当压力超过 6 MPa 时,土壤表面会出现不均匀的油斑,这对实验结果的影响较大。

## 3 参数分析及优化

### 3.1 激发能量和 CCD 相机接收参数分析

当光源能量较低时,荧光信号弱,低质量分数的样品不易被激发,不利于定量分析。当能量较高时,高质量分数样品的荧光可能达到饱和。因此,合适的光源能量和测试时间是实验的关键。经测试,本实验最终选择了 4 颗 LED 光源聚集共同激发样品。使用 CCD 相机来接收荧光,相机的镜头与样品之间的角度会影响荧光图像的收集。在实验中改变二者之间的角度,当相机镜头正对着样品,即二者间角度为 0° 时,获取到的图像荧光较强,如图 7 所示。在实验的过程中使用黑色遮光布对实验系统进行遮光处理,避免环境光的影响。

### 3.2 实验系统检测能力评价指标

检测限(LOD)、质量分数与荧光信号的相关性,以及系统稳定性是评价系统检测能力的重要指标。检测限为某特定方法在给定的置信度内可从样品中检出待测物质的最小质量分数,是衡量方法和仪器灵敏度

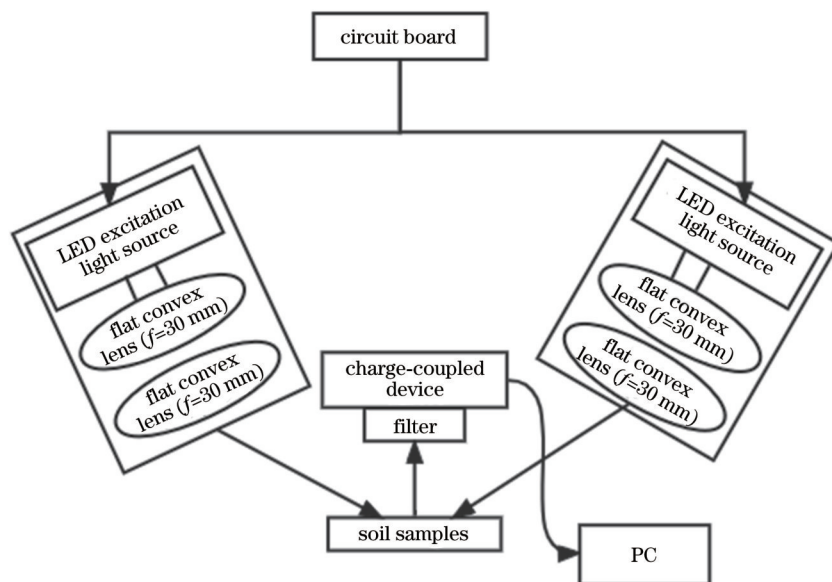


图 5 荧光检测系统示意图

Fig. 5 Schematic diagram of fluorescence detection system

表 1 含有不同质量分数机油的样品的配制

Table 1 Preparation of samples containing different mass fractions of oil

| Mass fraction of oil in soil / % | Mass of soil with 5% oil / g | Blank / g | Mass fraction of oil in soil / % | Mass of soil with 5% oil / g | Blank / g | Mass fraction of oil in soil / % | Mass of soil with 5% oil / g | Blank / g |
|----------------------------------|------------------------------|-----------|----------------------------------|------------------------------|-----------|----------------------------------|------------------------------|-----------|
| 0.1                              | 0.2                          | 9.8       | 1.0                              | 2.0                          | 8.0       | 1.9                              | 3.8                          | 6.2       |
| 0.2                              | 0.4                          | 9.6       | 1.1                              | 2.2                          | 7.8       | 2.0                              | 4.0                          | 6.0       |
| 0.3                              | 0.6                          | 9.4       | 1.2                              | 2.4                          | 7.6       | 2.1                              | 4.2                          | 5.8       |
| 0.4                              | 0.8                          | 9.2       | 1.3                              | 2.6                          | 7.4       | 2.2                              | 4.4                          | 5.6       |
| 0.5                              | 1.0                          | 9.0       | 1.4                              | 2.8                          | 7.2       | 2.3                              | 4.6                          | 5.4       |
| 0.6                              | 1.2                          | 8.8       | 1.5                              | 3.0                          | 7.0       | 2.4                              | 4.8                          | 5.2       |
| 0.7                              | 1.4                          | 8.6       | 1.6                              | 3.2                          | 6.8       | 2.5                              | 5.0                          | 5.0       |
| 0.8                              | 1.6                          | 8.4       | 1.7                              | 3.4                          | 6.6       |                                  |                              |           |
| 0.9                              | 1.8                          | 8.2       | 1.8                              | 3.6                          | 6.4       |                                  |                              |           |

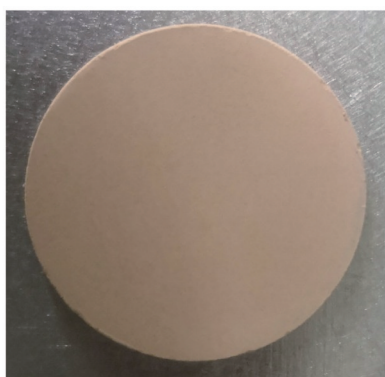


图 6 制备的土壤片实物图

Fig. 6 Physical picture of prepared soil sheet

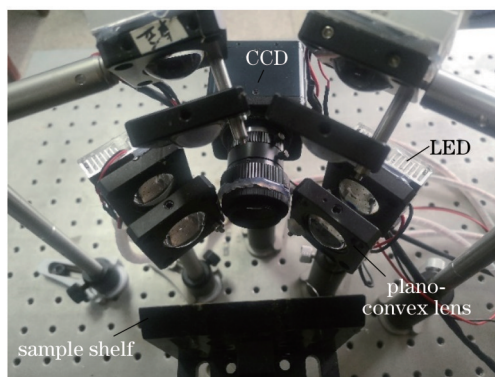


图 7 实验系统

Fig. 7 Experimental system

的重要指标之一。检测限的计算公式为

$$L_{OD} = \frac{K \cdot S_b}{M}, \quad (1)$$

式中:  $S_b$  为空白样信号的标准偏差(本研究中空白样品

重复测量 20 次);  $M$  为定标曲线的斜率;  $K$  为根据所需置信度选取的常数, 根据国际纯粹与应用化学联合会 (IUPAC) 对检测限的定义, 将该常数设为 3, 此时的置信度大约为 90%。

稳定性可以衡量系统是否可以稳定运行,采用相对标准偏差(RSD)作为判断标准。计算公式为

$$D_{RS} = \frac{\sqrt{\frac{\sum_{i=1}^n (x_i - \bar{x})^2}{n-1}}}{\bar{x}}, \quad (2)$$

式中: $n$ 为测量次数; $x_i$ 为第*i*次测得的值; $\bar{x}$ 为*n*次测量值的平均值。对同一质量分数的样品进行多次测试,求得的相对标准偏差越低,说明系统的稳定性越好。

## 4 数据分析

### 4.1 数据预处理

使用 CCD 相机获取到的图像为灰度图像,而灰度图像具有代表性的参数即为灰度值,因此选择分析光斑的灰度值作为信号值。具体方法为使用最大类间方差法获取相机拍到的原始图像的阈值并将其转化为二值图,亮的部分的数值为 1,暗的部分的数值为 0。该二值图与原始灰度图都是矩阵,且大小相同,将两个矩阵进行点乘操作,圆圈之外的数值均变为了 0,圆圈内的数值为灰度值数据。统计亮斑的像素点个数,用灰度值总和除以总个数,即可求得荧光灰度值的均值。在本实验中,均获取了各质量分数样品前 5 s 的荧光图像来进行分析,每隔 1 s 获取一张,共计 5 张。

利用阈值将原图像分成前景图像和背景图像,当取最佳阈值时,背景应该与前景差别最大,衡量差别的标准是最大类间方差,该方法对噪音和目标大小十分敏感,可对类间方差为单峰的图像产生较好的分割效果。前景和背景图像的方差  $g$  为

$$g = w_0 \cdot (u_0 - u)^2 + w_1 \cdot (u_1 - u)^2 = w_0 \cdot w_1 \cdot (u_1 - u_0)^2, \quad (3)$$

式中: $w_0$ 为前景点数占图像总点数的比例; $u_0$ 为前景点数的平均灰度; $w_1$ 为背景点数占图像总点数的比例; $u_1$ 为背景点数的平均灰度; $u$ 为整幅图像的灰度均值。方差最大时可以认为前景和背景差异最大,此时的灰度是最佳阈值。

在 CCD 相机采集图像的过程中,因受传感器材料属性、工作环境、电子元器件结构和电路结构等影响,会引入各种噪声。在图像信号传输过程中,由于传输介质和记录设备等存在的不完善,故数字图像在传输记录过程中往往会受到多种噪声污染。当部分前景目标被错分为背景或部分背景被错分为前景时,两个部分的差别均会变小,从而导致分割的错分概率变大,也会产生噪声。因此,对所有获取到的图像进行降噪处理,分别采用了高斯滤波和均值滤波降噪,处理后二者结果差别不大,但均值滤波易使图像模糊化,将图像中的边缘信息和特征信息模糊掉,故采用高斯降噪处理,并选取合适的滤波器大小和标准差。

高斯滤波器是一种线性滤波器,其卷积模板中的

系数会随着与模板中心距离的增大而减小。高斯滤波算法根据高斯函数选择滤波权值,具体过程为对一幅图片的像素值进行加权平均,滤波结果的像素值是由输入图片像素值与高斯滤波核矩阵进行相乘并累加后得到的,在数值上表现为平滑化。滤波过程的定义为

$$O(x, y) = \sum_{u=0}^{p-1} \sum_{v=0}^{q-1} I(u, v) G(u-x, v-y), \quad (4)$$

式中: $I(u, v)$ 是大小为  $p \times q$  的输入图片矩阵; $G(u, v)$ 为高斯函数; $O(x, y)$ 为输出结果矩阵。 $G(u, v)$ 的定义为

$$G(u, v) = \frac{1}{2\pi\sigma^2} \exp\left[-\frac{(u-u_0)^2 + (v-v_0)^2}{2\sigma^2}\right], \quad (5)$$

式中: $u_0$ 和  $v_0$ 为均值,一般取值为 0,  $(u_0, v_0)$ 为中心点坐标; $\sigma^2$ 为方差,表示高斯曲线的宽度。滤波器的大小是行列长度为奇数的方阵,取值由  $\sigma$  决定。一般根据具体图像情况,选择合适的滤波器大小与标准差。 $\sigma$  越大,高斯滤波器的频带就越宽,平滑程度就越好。经过测试,当选取的滤波器大小为  $5 \times 5$ ,滤波器的标准差为 1 时,效果最好。

### 4.2 系统稳定性测试

在对配制好的样品进行测试前,对空白样品进行测试,一方面可以判断系统的稳定性,另一方面可以计算出空白样品的标准偏差,以计算检测限。共测试了 20 次,荧光图像和数值分别如图 8 和表 2 所示。计算出 20 次样品测试的标准偏差为 0.060696,由此可见,系统的稳定性较强。



图 8 空白土壤样品荧光图

Fig. 8 Fluorescence image of blank soil sample

表 2 20 次空白样品测试结果

Table 2 Results of 20 blank sample tests

| Test No. | Value   | Test No. | Value   | Test No. | Value   | Test No. | Value   |
|----------|---------|----------|---------|----------|---------|----------|---------|
| 1        | 100.322 | 6        | 100.435 | 11       | 100.456 | 16       | 100.363 |
| 2        | 100.351 | 7        | 100.387 | 12       | 100.488 | 17       | 100.419 |
| 3        | 100.406 | 8        | 100.483 | 13       | 100.447 | 18       | 100.534 |
| 4        | 100.360 | 9        | 100.412 | 14       | 100.524 | 19       | 100.439 |
| 5        | 100.328 | 10       | 100.432 | 15       | 100.461 | 20       | 100.373 |

### 4.3 校正模型建立

对质量分数分别为 0.1%、0.6%、1.5%、1.9% 和 2.5% 的土壤样品每 1 s 获取 1 张图片, 获得的前 5 张图片, 如图 9 所示。对 5 s 内的荧光值求平均并建立定

标曲线, 如图 10 所示。质量分数和信号之间的相关系数 ( $R^2$ ) 为 0.9889, 即二者的相关性较强。计算得出检测限为

$$L_{\text{OD}} = \frac{3 \times 0.060696}{2215.7} \times 10^6 = 82.18. \quad (6)$$

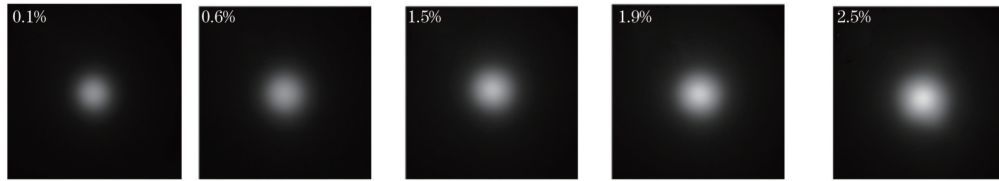


图 9 定标样品的荧光图像

Fig. 9 Fluorescence images of calibrated samples

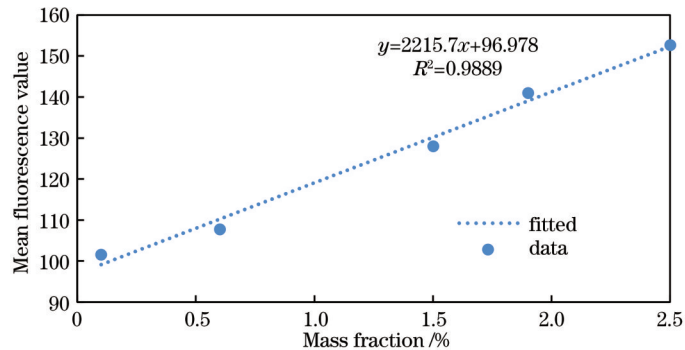


图 10 定标曲线

Fig. 10 Calibration curve

### 4.4 测试样质量分数反演

测试了质量分数为 0.2%、0.3%、0.4% 等 20 个土壤样品, 每 1 s 获取 1 张图片, 如图 11 所示, 获得前 5 张荧光图像的数据值如表 3。由建立的定标曲线可知,

方程为  $y = 2215.7x + 96.978$ , 将表 3 中样品荧光值的均值代入该方程, 可反演出质量分数值和误差, 如表 4 所示。

表 3 测试样品的荧光值均值

Table 3 Mean fluorescence values of test samples

| Mass fraction / % | 0.20    | 0.30    | 0.40    | 0.50    | 0.70    | 0.80    | 0.90    | 1.00    | 1.10    | 1.20    |
|-------------------|---------|---------|---------|---------|---------|---------|---------|---------|---------|---------|
| 1 s               | 103.591 | 106.261 | 106.766 | 108.372 | 111.059 | 116.711 | 120.969 | 122.033 | 126.043 | 124.553 |
| 2 s               | 103.513 | 106.032 | 106.805 | 107.786 | 110.792 | 115.417 | 119.132 | 121.410 | 123.827 | 124.182 |
| 3 s               | 103.555 | 105.84  | 106.819 | 106.683 | 110.701 | 114.259 | 119.451 | 120.236 | 122.073 | 123.595 |
| 4 s               | 103.478 | 105.596 | 106.737 | 106.449 | 110.478 | 113.839 | 116.119 | 119.765 | 120.593 | 122.460 |
| 5 s               | 103.484 | 104.688 | 106.837 | 106.314 | 110.401 | 113.659 | 115.624 | 119.462 | 120.015 | 121.861 |
| Average           | 103.524 | 105.683 | 106.793 | 107.121 | 110.686 | 114.777 | 118.259 | 120.581 | 122.510 | 123.330 |
| Mass fraction / % | 1.30    | 1.40    | 1.60    | 1.70    | 1.80    | 2.00    | 2.10    | 2.20    | 2.30    | 2.40    |
| 1 s               | 132.123 | 131.146 | 132.636 | 138.967 | 139.740 | 146.028 | 149.549 | 150.750 | 153.684 | 155.712 |
| 2 s               | 127.331 | 127.694 | 131.352 | 136.203 | 138.981 | 144.371 | 146.727 | 149.326 | 150.496 | 153.831 |
| 3 s               | 124.318 | 126.584 | 130.977 | 134.475 | 137.335 | 143.198 | 144.942 | 147.746 | 148.372 | 152.236 |
| 4 s               | 122.491 | 124.013 | 130.671 | 132.904 | 135.867 | 141.501 | 142.985 | 146.318 | 146.583 | 150.487 |
| 5 s               | 120.811 | 122.672 | 129.552 | 131.375 | 134.441 | 141.023 | 141.295 | 145.762 | 144.741 | 149.098 |
| Average           | 125.415 | 126.422 | 131.038 | 134.785 | 137.273 | 143.224 | 145.099 | 147.980 | 148.775 | 152.273 |

由表 4 可知, 样品反演的质量分数与实际测得的质量分数误差不大, 除了  $2000 \times 10^{-6}$  和  $3000 \times 10^{-6}$  两个低质量分数的样品噪声较大导致误差大外, 其余质

量分数样品的误差基本在 12% 内, 将测试样品的质量分数对应的数据带入到定标曲线中, 如图 12 所示。

表 4 测试样品的反演质量分数和误差

Table 4 Inversion mass fractions and deviations of test samples

| Mass fraction /<br>10 <sup>-6</sup> | Mean<br>fluorescence | Inversion /<br>10 <sup>-6</sup> | Deviation / % | Mass fraction /<br>10 <sup>-6</sup> | Mean<br>fluorescence | Inversion /<br>10 <sup>-6</sup> | Deviation / % |
|-------------------------------------|----------------------|---------------------------------|---------------|-------------------------------------|----------------------|---------------------------------|---------------|
| 2000                                | 103.524              | 2950                            | 47.728        | 13000                               | 125.415              | 12830                           | 1.275         |
| 3000                                | 105.683              | 3930                            | 30.961        | 14000                               | 126.422              | 13290                           | 5.081         |
| 4000                                | 106.793              | 4430                            | 10.740        | 16000                               | 131.038              | 15370                           | 3.925         |
| 5000                                | 107.121              | 4580                            | 8.448         | 17000                               | 134.785              | 17060                           | 0.371         |
| 7000                                | 110.686              | 6190                            | 11.617        | 18000                               | 137.273              | 18190                           | 1.033         |
| 8000                                | 114.777              | 8030                            | 0.413         | 20000                               | 143.224              | 20230                           | 4.360         |
| 9000                                | 118.259              | 9600                            | 6.718         | 21000                               | 145.099              | 20870                           | 3.420         |
| 10000                               | 120.581              | 10650                           | 6.527         | 22000                               | 147.980              | 21720                           | 4.630         |
| 11000                               | 122.510              | 11520                           | 4.758         | 23000                               | 148.775              | 23020                           | 1.640         |
| 12000                               | 123.330              | 11890                           | 0.888         | 24000                               | 152.273              | 23380                           | 3.983         |

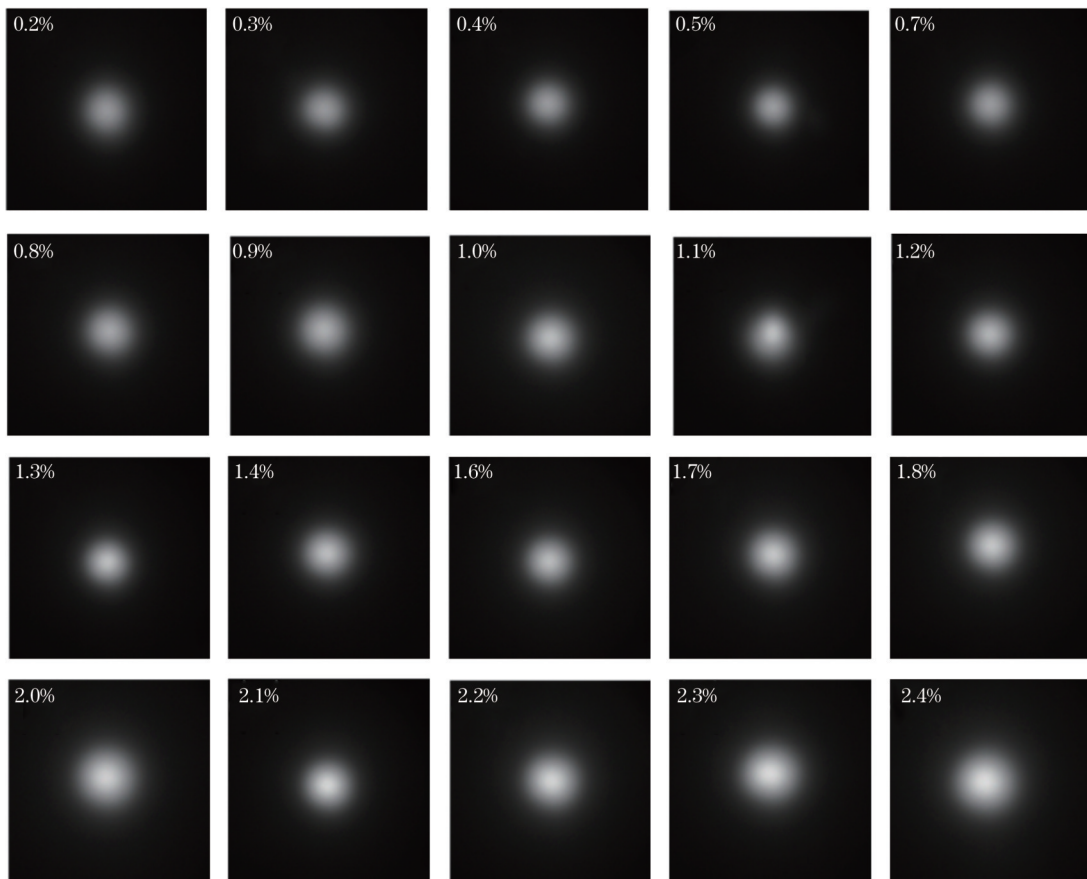


图 11 测试样品的荧光图像

Fig. 11 Fluorescence images of tested samples

## 5 结 论

荧光成像技术打破了传统有机物检测方法样品预处理复杂、测试速度慢等缺点,具有检测速度快、方便等特点。搭建了荧光成像探测实验系统,研究了土壤石油芳香烃总量快速直接测量方法,其精密度和准确度满足场地快速检测的需求。系统搭建过程中分析了光源的激发能量和 CCD 相机接收参数对荧光成像结

果的影响,由此选取了最优参数并优化了实验系统。基于实验系统获取了系列标准土壤机油芳香烃荧光图像,研究了图像信号处理方法,建立了校正模型,荧光图像信号与质量分数间的决定系数为 0.9889,检测限为 82.18。校正模型对测试样中机油芳香烃的测量误差基本在 12% 内。该研究为荧光成像原位监测技术应用于土壤石油芳香烃有机污染快速监测提供了方法基础,但对于低质量分数的样品,测量误差较大,该问

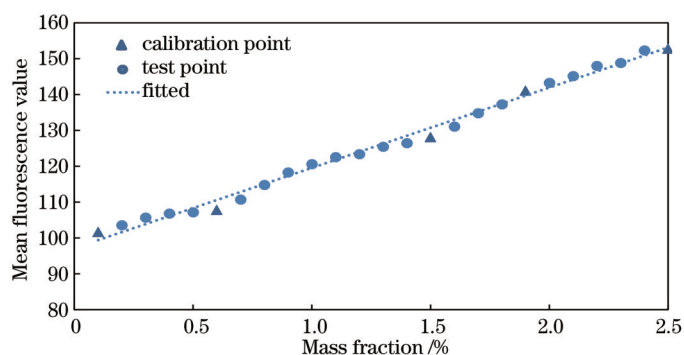


图 12 测试样品荧光值曲线

Fig. 12 Fluorescence value curve of test samples

题值得进一步探究。此外,正在深入研究土壤湿度、温度、pH值和有机质等理化参数对土壤石油芳香烃荧光图像信号的影响。

## 参 考 文 献

- [1] Ji Y Y, Gao F H, Wu Z H, et al. A review of atmospheric benzene homologues in China: characterization, health risk assessment, source identification and countermeasures[J]. *Journal of Environmental Sciences*, 2020, 95: 225-239.
- [2] Yang Z N, Liu Z S, Wang K H, et al. Soil microbiomes divergently respond to heavy metals and polycyclic aromatic hydrocarbons in contaminated industrial sites[J]. *Environmental Science and Ecotechnology*, 2022, 10: 100169.
- [3] 张万付. 东北地区农田土壤有机污染现状分析[J]. *现代农业*, 2018(5): 33-34.  
Zhang W F. Analysis of organic pollution of farmland soil in northeast China[J]. *Modern Agriculture*, 2018(5): 33-34.
- [4] Kim Y Y, Kim M K, Shin H S. Determination of volatile organic compounds (VOCs) levels from various smoking cessation aids by using gas chromatography-mass spectrometry methodology[J]. *Journal of Toxicology and Environmental Health, Part A*, 2022, 85(3): 110-120.
- [5] Halder S, Xie Z Z, Nantz M H, et al. Integration of a microconcentrator with solid-phase microextraction for analysis of trace volatile organic compounds by gas chromatography-mass spectrometry[J]. *Journal of Chromatography A*, 2022, 1673: 463083.
- [6] 陈国胜, 王少涵, 陈月媚, 等. 固相微萃取联用气相色谱-质谱法快速分析水中痕量苯系物[J]. *大学化学*, 2022, 37(5): 76-83.  
Chen G S, Wang S H, Chen Y M, et al. Rapid analysis of trace BTEX in water by solid phase microextraction coupled with gas chromatography-mass spectrometry[J]. *University Chemistry*, 2022, 37(5): 76-83.
- [7] Shen J, Liu B, Wu J, et al. Characterization of fluorescent dissolved organic matters in metalworking fluid by fluorescence excitation-emission matrix and high-performance liquid chromatography[J]. *Chemosphere*, 2020, 239: 124703.
- [8] Li T Y, Cao X C, He S H, et al. An accelerated solvent extraction and gas chromatography-flame ionization detector method to rapidly determining and assessing total petroleum hydrocarbon contamination in soil from Fushan oilfield, China [J]. *Environmental Science and Pollution Research*, 2020, 27 (30): 37444-37454.
- [9] 张世芝, 张明锦. 紫外光谱法结合化学计量学用于水中部分苯系物的同时测定[J]. *化学研究与应用*, 2020, 32(11): 1967-1972.  
Zhang S Z, Zhang M J. Ultraviolet spectroscopy combined with chemometrics for simultaneous determination of some benzene series in water[J]. *Chemical Research and Application*, 2020, 32 (11): 1967-1972.
- [10] 孟凡昊, 秦敏, 梁帅西, 等. 合肥市典型交通干道大气苯系物的特征分析[J]. *环境科学*, 2018, 39(9): 4060-4069.  
Meng F H, Qin M, Liang S X, et al. Characteristics of atmospheric BTX near a main road in Hefei City[J]. *Environmental Science*, 2018, 39(9): 4060-4069.
- [11] 王玉涛, 石辉, 刘雄飞, 等. 黄土丘陵区不同植被下土壤可溶性有机物的荧光特征研究[J]. *植物营养与肥料学报*, 2016, 22 (1): 171-179.  
Wang Y T, Shi H, Liu X F, et al. Spectrofluorometric characterization of soil dissolved organic matter under different vegetation in Loess Hilly Region[J]. *Journal of Plant Nutrition and Fertilizer*, 2016, 22(1): 171-179.
- [12] 庞燕华, 陈莉娜, 张晟, 等. 热处理后水稻土溶解性有机质光谱特征的变化[J]. *农业环境科学学报*, 2018, 37(3): 505-514.  
Pang Y H, Chen L N, Zhang S, et al. Changes in the spectral characteristics of dissolved organic matter from paddy soil after heating[J]. *Journal of Agro-Environment Science*, 2018, 37(3): 505-514.
- [13] Douglas R K, Nawar S, Alamar M C, et al. Rapid detection of alkanes and polycyclic aromatic hydrocarbons in oil-contaminated soil with visible near-infrared spectroscopy[J]. *European Journal of Soil Science*, 2019, 70(1): 140-150.
- [14] 吴嘉鹏, 楼振纲, 胡笑妍, 等. 紫外法与红外法测定石油类的比对研究[J]. *中国无机分析化学*, 2019, 9(6): 78-82.  
Wu J P, Lou Z G, Hu X Y, et al. Comparison of ultraviolet and infrared spectrophotometry in the determination of petroleum[J]. *Chinese Journal of Inorganic Analytical Chemistry*, 2019, 9(6): 78-82.



# Rapid Detection Method of Total Amount of Aromatic Hydrocarbons in Soil Based on Fluorescence Imaging Technology

Shi Gaoyong<sup>1,2,3</sup>, Yang Ruifang<sup>2,3\*</sup>, Zhao Nanjing<sup>2,3\*\*</sup>, Liu Liangchen<sup>1,2,3</sup>, Yang Jinqiang<sup>1,2,3</sup>,  
Huang Peng<sup>2,3,4</sup>, Yin Gaofang<sup>2,3</sup>, Fang Li<sup>2,3</sup>, Liu Wenqing<sup>2,3</sup>

<sup>1</sup>College of Environmental Science and Optoelectronic Technology, University of Science and Technology of China, Hefei 230026, Anhui, China;

<sup>2</sup>Key Laboratory of Environmental Optics and Technology, Anhui Institute of Optics and Fine Mechanics, Hefei Institutes of Physical Science, Chinese Academy of Sciences, Hefei 230031, Anhui, China;

<sup>3</sup>Key Laboratory of Optical Monitoring Technology for Environment of Anhui Province, Hefei 230031, Anhui, China;

<sup>4</sup>School of Biology, Food and Environment, Hefei University, Hefei 230601, Anhui, China

## Abstract

**Objective** With the rapid development of petrochemical and related industries, oil pollution incidents occur frequently. Aromatic hydrocarbons, benzene series, and polycyclic aromatic hydrocarbons are the main components of petroleum, which have effects of teratogenicity, carcinogenicity, and gene mutation. Once they enter the soil, they will accumulate in the soil for a long time and ultimately affect human health through the food chain. The traditional detection techniques of organic pollutants mainly include gas chromatography, gas chromatography-mass spectrometry, liquid chromatography, etc. Although these methods are standard methods with high sensitivity and excellent accuracy, they have the disadvantages of complex sample pretreatment and slow test speed and are not suitable for rapid on-site detection. At present, the existing optical detection techniques mainly detect the components of organic matter, and the measured components have large errors. In addition, the total amount of organic matter cannot be simply summed. Imaging technology provides an alternative way to realize the total detection of soil organic pollutants. In this paper, an ultraviolet-induced fluorescence imaging system is built, and the direct detection method of the total amount of aromatic hydrocarbons in standard soil is studied, which provides feasibility for the rapid determination of the total amount of aromatic hydrocarbons in soil.

**Methods** The experimental system is built using a light emitting diode (LED) excitation light source, plano-convex lens, filter, CCD camera, sample holder, control circuit board, and personal computer. After the excitation light from the LED light source is collimated and converged by the lens group, it is irradiated on the surface of the soil sample with a certain size of the light spot, and the aromatic hydrocarbons in the soil are excited to generate fluorescence. After the CCD camera captures the fluorescent image signals, the signals are transmitted to the computer for analysis and processing. A standard soil (GBW07494) is selected to prepare the experimental samples of motor oil (15W-40). The original image captured by the camera is obtained by using the maximum inter-class variance method to obtain the image threshold and converted into a binary image, and the binary image is dot multiplied with original gray image to obtain the gray value data.

**Results and Discussions** Aiming at the problem of rapid detection of the total amount of aromatic hydrocarbons in soil, methods such as the acquisition of aromatic hydrocarbon fluorescence signals in soil, feature extraction, and total concentration inversion based on fluorescence imaging technology are studied. On the basis of an LED ultraviolet excitation light source, area-scanning CCD camera, lens, and other devices, an experimental system is built. The parameters such as the optimal excitation energy and excitation angle of the light source are obtained, and the detection capability of the experimental system is analyzed. Through this experimental system, a series of fluorescence images of petroleum in standard soil with mass fraction ranging from 0 to  $25000 \times 10^{-6}$  are obtained. Based on the Gaussian noise reduction and maximum inter-class variance method, the image noise suppression and fluorescence signal extraction methods are studied, and an inversion model of the total amount of aromatic hydrocarbons in standard soil is established. Furthermore, the total amount of aromatic hydrocarbons in the sample to be tested is predicted by using the inversion model. The results show that the coefficient of determination ( $R^2$ ) of the total inversion model reaches 0.9889 (Fig. 10), and the detection limit is 82.18. For 20 samples, the errors are basically within 12%.

**Conclusions** Fluorescence imaging technology breaks through the shortcomings of traditional organic detection methods such as complex sample preprocessing and slow testing speed, and has the characteristics of fast and convenient detection. In this paper, a fluorescence imaging detection experimental system is built, and a rapid and direct measurement method of

the total amount of aromatic hydrocarbons in soil is studied. Its precision and accuracy have met the needs of rapid field detection. In the process of system construction, the influence of the excitation energy of the light source and the receiving parameters of the CCD camera on the fluorescence imaging results is analyzed, and the optimal parameters are selected, with the experimental system optimized. Based on the experimental system, a series of aromatic hydrocarbon fluorescence images for petroleum in standard soil are obtained. The image signal processing method is studied, and a calibration model is established. The coefficient of determination between the fluorescence image signal and the mass concentration is 0.9889, and the detection limit is 82.18. This study provides a method basis for the application of fluorescence imaging *in situ* monitoring technology to the rapid monitoring of organic pollution of aromatic hydrocarbons in soil. In addition, the effects of physical and chemical parameters such as soil moisture, temperature, pH, and organic matter on the fluorescence image signals of aromatic hydrocarbons in soil are being studied in depth.

**Key words** measurement; soil; fluorescence imaging; polycyclic aromatic hydrocarbons; cameras; image processing